Published in Physical Review B 59, issue 24, 15975-15989, 1999
which should be used for any reference to this work

Experimental evidence for kinetically determined intermixed Volmer-Weber growth in thin-film deposition of Au on Ag(110)

J. Hayoz,* Th. Pillo, R. Fasel, L. Schlapbach, and P. Aebi
Institut de Physique, Université de Fribourg, Pérolles, CH-1700 Fribourg, Switzerland

Au films, from the submonolayer range up to 11 ML, have been deposited *in situ* at 300 K. The geometrical structures of these films have been investigated combining full-hemispherical x-ray photoelectron diffraction, low-energy electron diffraction (LEED), low-energy ion-scattering spectroscopy, and scanning tunneling microscopy leading to an intermixed Volmer-Weber growth model. The results demonstrate that below 0.5 ML most Au atoms are buried within the second substrate layer, forming inverted Ag/Au areas on the surface. The ejected Ag atoms and vacancies created during the Au-Ag exchange nucleate into elongated two-dimensional Ag islands and vacancy clusters, respectively, quickly breaking up the surface into smaller terraces. Above about 0.5-ML coverage, the Au-Ag exchange mechanism continues to be active. In addition, due to the reduced mobility of Au atoms deposited on inverted Ag/Au areas, one-dimensional Au stripes as well as elongated three-dimensional (1×3)-symmetric Au islands are observed already at submonolayer coverages on inverted Ag/Au areas. Only after the deposition of more than 8-ML Au is the Ag substrate completely covered, and missing-row reconstructed terraces extend over regions large enough to yield a well-defined 1×2 LEED pattern. The growth model is compared to both, published thermodynamic equilibrium predictions and molecular-dynamics simulations, revealing that the Au/Ag(110) growth system is kinetically determined.

I. INTRODUCTION

Thin films are of interest from many different points of view.[1] They are technologically important in optical coatings, corrosion protection, and semiconductor devices. Many of these applications involve increasingly complex and sophisticated growth processes. Thin films are also important within physical science itself in exploring differences between three-dimensional (3D) and (quasi-) two-dimensional (2D) states of matter. The intense research activity aimed at the growth of high-quality superlattices and multilayers has resulted in discoveries of physical phenomena such as the oscillatory magnetic interlayer coupling[2] and the giant magneto resistance effect.[3] These phenomena, however, depend strongly on the interface and film quality. One goal of interface and thin-film science, therefore, is to understand the growth process in sufficient detail to manipulate the structure and interface of the film, permitting improvement in thin-film devices.

Predicting the morphology and atomic arrangement of a thin film grown on a single-crystal substrate has been a continuing challenge. For epitaxy without intermixing at the interface, the growth is usually classified into three modes: 2D layer-by-layer growth, 3D crystallite formation, and layer-by-layer growth followed by 3D crystallite formation. These growth modes are known as the Frank–van der Merwe, Volmer-Weber (VW), and Stranski-Krastanov (SK) modes, respectively. Based on simple thermodynamical arguments the growth mode can be predicted, or at least discussed, using Bauer's criteria.[4] Growth in two dimensions is preferred if the sum of the surface-free energy of the adsorbate (γ_a) and the interface-free energy (γ_i) is smaller than the substrate-free energy (γ_s). The SK mode is the intermediate case, where this energetic difference changes sign at a critical layer thickness provoking a transition from 2D to 3D growth. The interface energy γ_i is usually an unknown quantity. An order-of-magnitude estimate can sometimes be obtained from bulk alloy heat of formation data. Such a simple energetic picture has to be refined for heteroepitaxy by taking into account the strain energy arising from lattice mismatch (LM).[5] In order to reduce stress, systems with a large LM usually undergo structural transformations. This may end up with a change of the crystallographic orientation of the overlayer.[6]

To complicate matters further, one has to account for interface mixing, caused either by a surface-driven mechanism or a tendency for bulk alloy formation. Examples of such systems are as follows: (1) Au-Cu(001) (Ref. 7): for 0.5 ML of Au deposited on Cu(001), a 2D ordered $c(2\times2)$ Au-Cu monolayer is formed. (2) Au-Pt(110) (Ref. 8): at submonolayer coverages, most Au atoms are found in the second layer below the surface. (3) Au-Ni(110) (Ref. 9): here a 2D alloy is formed at low coverages even though the bulk materials are not miscible. The common characteristic of all these systems was a large LM. A criterion to evaluate the intermixing behavior of a system was discussed by Tersoff.[10] In a theoretical work based on surface, interface, and strain energy, he showed that mixing confined to a single atomic layer at the surface is expected quite generally for pairs of elements dominated by a large LM, even if they are immiscible in the bulk. Furthermore, in a very recent theoretical study an interface mixing energy (IFME) was defined as a measure of the thermodynamic stability of metallic interfaces, and a relation between bulk mixing energies and the IFME was proposed.[11] The advantage of this relation is that it gives the possibility to use available bulk data to estimate interface stabilities.

Vapor deposition experiments of the type considered here are nonequilibrium kinetic phenomena. Kinetic considerations—affected by temperature, deposition rate, and activation barriers—may play a dominant role over equilibrium thermodynamics.[1] The final state of the system depends on the microscopic pathway taken by the system, and is not necessarily the most stable. It may be determined kinetically. In general, certain parts of the overall process may be kinetically forbidden (e.g., dissolution into the substrate), others may be in ''local'' thermodynamic equilibrium, and some will be kinetically rate limiting. The degree to which growth proceeds away from equilibrium, therefore, decides to which extent the morphology will be determined by thermodynamic quantities, such as surface and interface energies, or by the growth kinetics. Molecular-dynamics (MD) simulations are known as a powerful tool to model kinetics of early film growth.[12] However, such simulations are still sufficiently approximate that the guidance and validation provided by experiments are necessary.

The Au/Ag interface is of technological relevance in the electronics industry, where aluminum electrodes on integrated circuits are usually interconnected with external, Ag coated lead frames by means of ultrasonic gold wire bonding.[13] In order to optimize the ultrasonic wire bonding parameters, a detailed understanding of the interface formation process is required. In collaboration with Schneuwly *et al.*[13] various aspects of the Au/Ag wire bonding system were studied, including its tribology, the influence of contamination on bonding contact quality, and the modification of the geometrical and electronic structure upon vapor deposition of Au on clean Ag single crystals at various temperatures. Finally, combining all information, a device based on thermoelectric temperature measurements was developed.[13] It turned out to be a powerful tool to carry out bondability analysis of so-called bond pats. Here, however, we focus only on the geometrical structure of the room-temperature (RT) growth of Au on the clean Ag(110) surface. Results concerning the electronic structure are published elsewhere.[14]

Over the entire range of composition, Au and Ag form a single face-centered-cubic (fcc) solid solution, the so-called electrum,[15] with a phase diagram showing no major complexities.[16] The complete miscibility is caused by the close chemical and physical similarities of the two metals: Au and Ag have an almost perfect lattice match, comparable surface energies (Ag has an about 21% lower surface energy than Au), and similar electronic and structural properties because they are isoelectronic. There are, however, some differences, and one of these is evident in that the three low-index surfaces of Au reconstruct, while those of silver do not.[17] It is obvious that upon reconstruction the surface energy changes and therefore the reconstruction may have a strong impact on the growth mode. Moreover, the IFME calculated for one single Ag_xAu_{1-x} alloy layer sandwiched between a Ag and a Au crystal predicts the interface to be unstable for the three low-index faces.[11] However, due to the very small RT diffusion coefficient $D_{300\,\mathrm{K}}=5.5\times10^{-16}$ Å^2/sec of Au impurities in pure Ag,[18] a thin Au film grown on a Ag crystal is not expected to dissolve into the Ag bulk at RT.

For the RT growth of Au on Ag(110), rather unconventional and controversial growth patterns have been reported. Using medium-energy ion scattering (MEIS), Fenter and Gustafsson[19] found that in the initial growth process, half of the Au atoms occupy second-layer sites, leaving about half of the Ag surface uncovered at 1-ML Au coverage. After a quantitative data analysis, intermixing at the interface was excluded, and the experimental observation was interpreted in terms of spontaneous Au-bilayer formation beginning in the submonolayer regime of Au coverages. Rousset *et al.*[20] subsequently performed a scanning tunneling microscopy (STM) study of this system. Below 1 ML they observed 2D finger growth starting from monoatomic steps and giving rise to anisotropic 3D islands upon further Au deposition (>1 ML). In contradiction to Fenter's Au-bilayer model, no evidence for islands and biatomic steps at submonolayer Au coverages was found. By reanalyzing the MEIS data of Ref. 19, Rousset *et al.* demonstrated that the MEIS results are also consistent with an interdiffusion picture. Their model states that the first ML of Au deposited on Ag(110) burrows below the surface, with the topmost surface layer consisting almost entirely of Ag atoms. For higher coverages, nearly pure Au islands elongated along $[\bar{1}10]$ then grow on top of this inverted Ag/Au layer.[20] Another STM investigation considering exclusively submonolayer Au coverages is only consistent with the STM data of Ref. 20 in the point that no biatomic steps are found.[21] The topographic features—islands and holes on terraces—however, are surprisingly different. Growth of 2D fingers as reported in Ref. 20 could only be observed when Au was deposited at 50 °C or higher. However, due to the absence of biatomic steps, the inverted Ag/Au-layer interpretation may also account for the STM data of Ref. 21. Further support for atomic exchange in the submonolayer regime is given by the surface core-level spectroscopy study of Hirschorn *et al.*[22] In contradiction to the previous interpretations,[19,20] the authors of Ref. 22 proposed the growth to proceed nearly layer by layer. They stated that the atomic exchange mechanism continues for multilayer coverages and reduces the content of Ag remaining in the top surface layer by 11% for the growth of each additional layer.

A further experimental inconsistency concerns the observed surface symmetries during Au deposition. On the one hand, Fenter and Gustafsson reported that Au films exhibit a 1×3 low-energy electron-diffraction (LEED) pattern at coverages between the 1×1 and 1×2 structures,[19] i.e., in the range from 3.6 up to 7 ML. On the other hand Hirschorn *et al.* state that 1×2 half-order spots emerge at 0.5-ML Au coverage, steadily becoming stronger with increasing Au coverage.[22]

Both the experimental inconsistencies and the unusual observed growth patterns attracted the interest of theorists over the last decade. In several theoretical investigations the heats of formation per atom of relaxed ideal configurations were predicted using the embedded-atom method (EAM),[23] the surface embedded-atom method (SEAM),[12] and density-functional theory calculations (DFT).[24] An overview of these theoretical findings is given in Table II of Ref. 12. SEAM and DFT agree in that the most favorable configuration for 1-ML coverage is for one Au layer to burrow one layer into the surface. Both calculations also agree that alloying in the second layer is favorable for 0.5-ML coverage, and that single-layer growth is preferred to Au-bilayer formation on

the surface. These results therefore are largely consistent with the inverted Ag/Au-layer interpretation.[20,22] On the other hand, the EAM potential favors burying the Au layer two layers deep, and also favors initial Au-bilayer over layer-by-layer growth on the surface. Additionally, the SEAM potential predicts that the configuration for 2-ML coverage is for the two Au layers to be buried below one layer of Ag. Further theoretical support for the inverted Ag/Au-layer configuration is given by Nieminen's atomic exchange mean-field (AEMF) study.[25] Using the Sutton-Chen potential, he predicted that at 1 ML the top layer is virtually of pure Ag and the Au concentration of the second layer is 85%. When increasing the Au coverage up to 4 ML, further interdiffusion is not favorable, but Au atoms tend to stay in the top layers forming clusters virtually free of Ag, at 2 and 3 ML ''preferring '' the 1×2 structure and above 3 ML the 1×3 structure. Finally, it is worth noting that the MD simulations performed by Haftel *et al.*[12] found that at 1-ML Au coverage the adlayer contains 30% of the deposited Au atoms, and with most (about 75%) of the buried Au atoms located within the original top substrate layer. In agreement with Ref. 25 MD simulations subsequently prefer the growth to become more 3D, resembling a 1×3 missing-row (MR) reconstruction at 3 ML, with the top layers containing higher proportions of Au atoms.

The aim of the present work is to clarify the present controversial situation for the RT growth of Au on Ag(110) and, consequently, to provide experimental data for the validation of theoretical predictions. Therefore, we investigated the geometric structure of 20 Au films ranging from 0.1 to 11 ML by means of x-ray photoelectron diffraction (XPD), LEED, low-energy ion-scattering (LE-ISS), and STM *in situ* and on the very same samples. We demonstrate that the combination of these four very surface-sensitive methods allows a detailed description of the growth process. For the lowest coverages a direct confirmation of the inverted Ag/Au-layer configuration was possible. The film morphology is strongly influenced by the anisotropic diffusion of vacancies, of replaced Ag atoms and of Au atoms deposited on inverted Ag/Au areas. The introduction of the 1×2 MR reconstruction, well known for clean Au(110) surfaces,[17] was carefully monitored upon Au deposition. Since the surface energy will change with the introduction of a surface reconstruction, it is interesting to observe how and when the transformation from the unreconstructed to the reconstructed phase takes place. A growth model based on all the information will be compared to thermodynamic equilibrium predictions,[12,23–25] as well as to results obtained from MD simulations.[12] This comparison reveals that the final state of the growth process is strongly kinetically influenced. In order to study the stability of the Au films, the dissolution behavior of the Au films into the Ag bulk was investigated upon annealing.

The paper is organized as follows. In Sec. II, experimental and data analysis procedures are described. Section III presents and discusses our experimental results with reference to previous experimental results. In Sec. IV, we propose a growth model based on the information gained from our experiments and compare it to theoretical studies. Finally, we summarize our findings in Sec. V.

II. EXPERIMENT

A. Experimental procedures

XPD has been chosen because of its chemical sensitivity and its sensitivity to local real-space order. It is a powerful technique for surface structural investigations,[26] and it has been shown that full-hemispherical XPD patterns provide very direct information about the near-surface structure. XPD is particularly attractive for structural investigations of adsorbate systems, epitaxial growth, interdiffusion at the surface, and structural phase transitions.[6–8,27–33] At photoelectron kinetic energies above about 500 eV, the strongly anisotropic scattering by the ion cores leads to a forward focusing of the electron flux along the emitter-scatterer axis. The photoelectron angular distribution, therefore, is to a first approximation a forward-projected image of the atomic structure around the photoemitters. LEED, in contrast, shows the symmetry of reciprocal space, is not chemically selective, and contains information about the long-range order of the atoms near the surface.

The scattering technique LE-ISS is a powerful tool for surface characterization. Bombarding a surface with noble-gas ions of some hundreds of eV, and measuring the energy and angular distributions of the recoiled ions, the elemental composition and the structure can be determined. LE-ISS is unique in that it is one of the very few techniques that probes the topmost layer exclusively.[34,35] Elastic scattering of the incoming ions from the first layer is the prevalent mechanism for their change in energy and momentum. Hence for a given scattering angle, the final energy of a scattered ion is directly related to the mass of the target atom. By acquiring energy spectra of the reflected ions an elemental analysis of the surface layer can be carried out. The exclusive first atomic layer sensitivity basically results from severe neutralization of primary noble-gas ions penetrating to deeper layers. Practically all incident ions, which stay too long in the vicinity of the surface either by undergoing multiple collisions or by penetrating to the second or deeper layers, leave the surface as neutrals and are not detected by an electrostatic energy analyzer.[34,35]

While diffraction and scattering techniques give access to a statistical average of the surface, STM, finally, probes its local topography. However, even with atomic resolution, it is almost impossible to distinguish different species on the surface with this technique.

The experiments were performed in a Vacuum Generators ESCALAB Mk II spectrometer modified for motorized sequential angle-scanning data acquisition,[36] equipped with a three-channeltron hemispherical electrostatic energy analyzer and with a base pressure in the low-10^{-11}-mbar region. Photoelectron spectra and diffraction patterns were measured using Mg $K\alpha$ ($h\nu=1253.4$ eV) radiation. The He^+ ion beam used for the LE-ISS experiment was produced by a VG AG 60-185 Ion Gun with a nominal angular spread of 0.2°. During operation, a liquid-nitrogen trap is activated on the He line in order to purge the He gas (99.997% pureness) from residual impurities. The relative angle between the fixed ion gun and the analyzer is 142° defining the scattering angle θ_{sc}. STM experiments were performed with a DME[37] Rasterscope 3000 using always the same electrochemically etched W tip. All images were acquired in a constant current

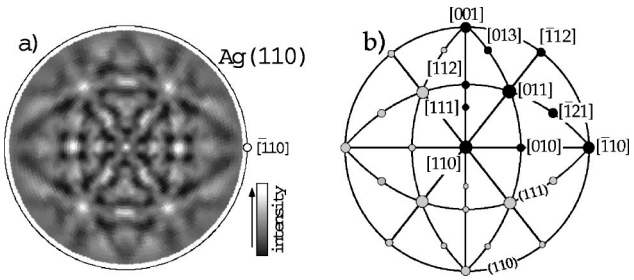

FIG. 1. (a) Stereographic projection of the Mg K_α exited Ag $3d_{5/2}$ photoelectron ($E_{kin}=885.5$ eV) distribution for the clean Ag(110) surface. (b) Stereographic projection of low-index crystal directions (spots) and dense crystal planes (lines) for the (110) face of a fcc crystal serving as a guide for diffractograms shown in this work. The labeled low-index directions correspond to the black spots. Shaded spots represent equivalent directions.

mode, mainly with a negative sample voltage from 8 mV to 1.5 V and a tunneling current from 0.5 to 3 nA. All measurements, if not otherwise specified, have been performed at RT.

Clean Ag(110) surfaces have been prepared by cycles of 1.5-keV Ar^+ sputtering and annealing to 750 K. As a result, no C or O contaminations could be detected with x-ray photoelectron spectroscopy (XPS) and LEED displayed well-defined and sharp 1×1 spots. Care was taken to ensure that the Ag(110) sample reached RT before Au deposition. Au was deposited from a liquid-nitrogen-cooled hot-filament evaporator using a 0.3-mm molybdenum wire with a 0.09-mm Au wire wrapped around it, at pressures below 4×10^{-10} mbar. During Au deposition the film thickness was controlled by means of a water-cooled quartz oscillator. LEED pictures at different energies were taken for each film. After Au deposition, no contamination could be detected with XPS.

The sample was then transferred *in situ* to a two-axis goniometer which enables sweeping the photoelectron emission direction over the whole hemisphere above the surface by computer-controlled crystal rotation. For each Au film, so-called diffractograms of the Au $4f_{7/2}$ ($E_{kin}=1170.0$ eV) and the Ag $3d_{5/2}$ emission ($E_{kin}=885.5$ eV) were measured. The data-acquisition procedure for obtaining these diffractograms consists of measuring series of azimuthal (ϕ) scans, at polar angle intervals of $\triangle\theta=2°$. It begins at $\theta_{start}=88°$ off normal, and terminates at $\theta_{end}=0°$. The azimuthal angular step size at any polar angle is chosen such that the solid-angle sampling density is uniform. The resulting two-dimensional data $I(\theta,\phi)$, containing 5044 different angular settings, are visualized, in the form of a gray-scale image, through a stereographic projection [Fig. 1(a)]. Typical data-acquisition times were 8 h at a pressure of 4×10^{-11} mbar. Subsequently, the sample was transferred to the STM and, thereafter, the ion-scattering experiment was performed. After all these experiments, i.e., about 20 h after Au deposition, no contamination could be detected with XPS and no significant changes of the Au $4d$ to Ag $3d$ ratio was observed. Therefore, no significant dissolution of Au into the Ag bulk occurred at RT on the time scale of our experiments. Finally, in order to investigate the dissolution of the Au films into the Ag bulk the Au $4d$ to Ag $3d$ ratio was measured during annealing the Au films.

B. Data analysis

To model the growth of Au on Ag(110), an exact knowledge of the Au quantity deposited on the Ag(110) surfaces is important. In this study the number of deposited Au ML's was determined by calibrating the quartz oscillator reading (Q) using core-level spectroscopy (Au $4d$ to Ag $3d$ ratio). As will be demonstrated below, our XPD and LE-ISS data reveal that, for Q below a certain value Q_o, almost all Au atoms are found in the second layer. Then, taking into account this inverted Ag/Au configuration, the inelastic mean free path of the photoelectrons,[38] the analyzer transmission function as well as the photoionization cross sections, one can calculate the nominal number of deposited Au layers. Since the quartz oscillator reading is independent of the growth process, the resulting linear relation ML(Q) found for $Q\leqslant Q_o$ can be extended to all Q values.

In order to facilitate the discussion of the XPD data, in Fig. 1(b) we show the stereographic projection of the main low-index directions and high-density crystal planes for the fcc(110) crystal surface, together with the experimental Ag $3d_{5/2}$ XPD pattern as obtained from the clean Ag(110) surface [Fig. 1(a)]. Intensity maxima and bands appear at locations of low-index directions and high-density atomic planes, respectively. Note that the center of the circle corresponds to the surface normal while the outer circle represents angles parallel to the surface, i.e., 90° off normal. All diffractograms, LEED patterns, and STM images we present in this paper are oriented such that the [$\bar{1}$10] direction of the underlying Ag(110) crystal points to the right-hand side, as is the case in Fig. 1. For each of the 5044 angular settings, the total intensity was recorded at the kinetic energy corresponding to the maximum of the relevant peak (I_{peak}) and at its high-energy footpoint (I_{high}). The background-corrected intensity was then calculated by subtracting I_{high} from I_{peak}. The patterns have been azimuthally averaged exploiting the twofold rotational symmetry of the Ag(110) substrate, and normalized to a smooth polar angle-dependent background.

In LE-ISS, as in any scattering experiment, the scattered ion intensity I is proportional to the primary ion intensity I_o, the number of scattering centers n, and the cross section $d\sigma$.[34,35] Taking into account our scattering geometry ($\theta_{sc}=142°$) and the selected primary ion energy ($E_o=2$ keV), we calculated the scattering cross sections for scattering at Au atoms ($d\sigma_{\mathrm{Au}}$) and Ag atoms ($d\sigma_{\mathrm{Ag}}$), respectively, using the Molière potential.[34,35] Besides depending on the scattering cross section, the backscattered intensity I essentially depends on the ion neutralization probability P. The $P_{\mathrm{Au}}/P_{\mathrm{Ag}}$ ratio, i.e., the ratio of the ion neutralization probabilities for scattering at Au and Ag atoms, respectively, was estimated experimentally.[39] The intensities of He-ions backscattered from Ag atoms (I_{Ag}) and Au atoms (I_{Au}), were determined by fitting the LE-ISS data with two asymmetric Lorentz functions (solid line in Fig. 2). Information on the quantitative surface composition, finally, is obtained from the ratio, v, between the number of Au atoms (n_{Au}) and the number of Ag atoms (n_{Ag}) probed by the ion beam. Based on the considerations discussed above, we find

$$v:=\frac{n_{\mathrm{Au}}}{n_{\mathrm{Ag}}}=\frac{P_{\mathrm{Ag}}d\sigma_{\mathrm{Ag}}I_{\mathrm{Au}}}{P_{\mathrm{Au}}d\sigma_{\mathrm{Au}}I_{\mathrm{Ag}}}=0.71\frac{I_{\mathrm{Au}}}{I_{\mathrm{Ag}}}. \quad (1)$$

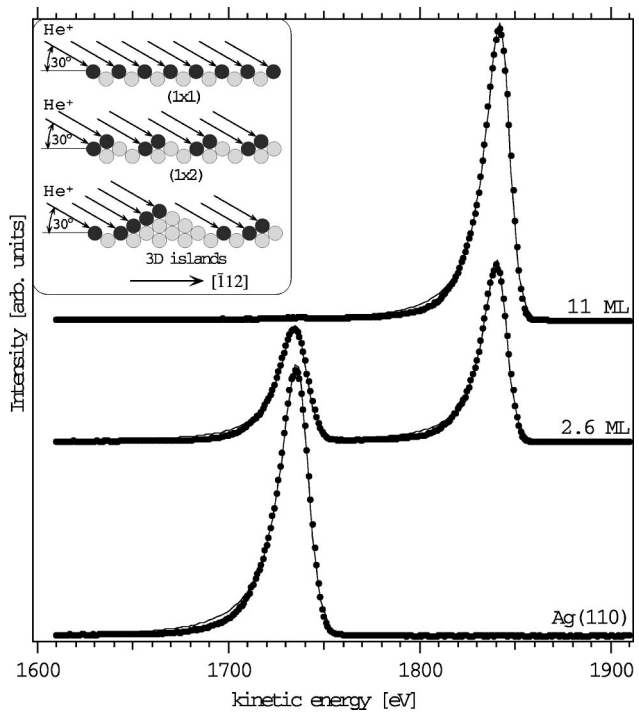

FIG. 2. LE-ISS spectra as obtained from the clean Ag(110) surface, covered with 2.6- and 11-ML Au, respectively. The solid lines are the best fits to the spectra using two asymmetric Lorentz functions. The spectra were measured using He^+ ions (the primary energy is $E_o = 2$ keV) incident along the $[0\bar{1}1]$ direction, i.e., the ion incidence direction was set to 30° off surface within a {111}-type scattering plane (arrows). The inset shows side views of the $[\bar{1}22]$ azimuth for three different surface terminations. Assuming top layer sensitivity, the filled circles correspond to the atoms probed by the He^+ ions, while the atoms drawn in a lighter shading are not exposed to the ion beam.

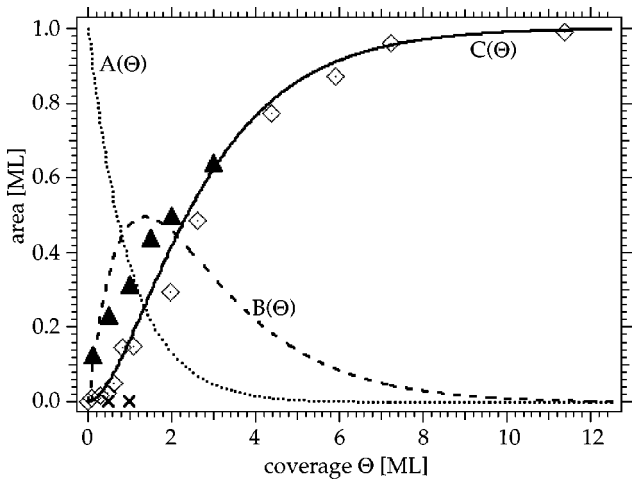

FIG. 3. Au surface concentration n_{Au} (open diamonds) as a function of the Au coverage Θ. The solid curve $[C(\Theta)]$ is the best fit to the data using our growth model and was achieved with $k = 0.52$ (see Sec. IV). The dotted $[A(\Theta)]$ curve and the hairline $[B(\Theta)]$ curve show the evolution of bare Ag-bulk areas and inverted Ag/Au areas, respectively. The filled triangles and crosses correspond to the Au surface concentration as predicted by MD simulations (Ref. 12) and thermodynamic equilibrium modeling (Refs. 12 and 23–25).

III. EXPERIMENTAL RESULTS AND DISCUSSION

A. LE-ISS experiments

Figure 2 displays LE-ISS data measured on the clean unreconstructed Ag(110) surface (bottom curve) and on the 11-ML Au/Ag(110) sample (top curve). As will be shown below, the surface of the 11-ML-thick Au film is 1×2 MR reconstructed. The curve in the middle of Fig. 2 corresponds to the spectrum of a 2.6-ML-thick Au film and is an illustrative example for intermediate Au coverages. The spectra of Fig. 2 were measured in a {111}-type scattering plane with the ion incidence polar angle Ψ_{in} (with respect to the surface) fixed to 30°, i.e., the ion incidence direction is parallel to $\langle 0\bar{1}1\rangle$-type directions. In the case of an ideal unreconstructed fcc(110) surface ions incident along $[0\bar{1}1]$ exclusively probe the top layer atoms (see inset of Fig. 2). Upon formation of a 1×2 MR reconstruction half of the second layer atoms, for 3D island formation even parts of deeper layers become exposed to the ion beam. (Note that the definition of ''surface'' involves atoms from different layers for different structures.) However, the ion beam exclusively probes the projection of the surface parallel to the incidence direction on a plane perpendicular to the ion incidence direction (filled circles in insets of Fig. 2). Therefore, for the selected ion incidence direction the total number of atoms (n_{tot}) probed by the ion beam is not modified upon such surface transformations and n_{tot} always equals 1 ML. Au and Ag have almost identical lattice constants and therefore the number of atoms per layer is identical for these two elements. From these considerations it follows that the sum of n_{Au} and n_{Ag} equals to one ML for all Au coverages. Using the measured v [Eq. (1)] we find for n_{Au}:

$$n_{\mathrm{Au}}[ML] = \frac{v}{1+v}. \tag{2}$$

The open markers (diamonds) of Fig. 3 show n_{Au} as obtained for ions incident along $[0\bar{1}1]$ as a function of the Au coverage calibrated as described in Sec. II B. Assuming the composition of possible 3D structures on average to follow the twofold symmetry of the substrate, we consider n_{Au} to be a very good measure of the Au surface concentration. Hence $n_{\mathrm{Au}} = 0$ corresponds to a pure Ag surface, while $n_{\mathrm{Au}} = 1$ describes a pure Au surface. The solid curve $[C(\Theta)]$ of Fig. 3 represents the best fit to n_{Au} using the growth model discussed in Sec. IV. The growth model also accounts for the evolution of bare Ag-bulk areas $A(\Theta)$ (dotted curve) and inverted Ag/Au areas $B(\Theta)$ (hairline curve). The filled triangles and crosses indicate concentrations as predicted by MD simulations[12] and thermodynamic equilibrium modeling,[12,23–25] respectively.

Most importantly, we note that almost no Au atoms are detected at the surface for coverages below 0.5 ML. This is indicative, that at this point most of the deposited Au atoms are buried below the surface. The abrupt increase of n_{Au} at about 0.5 ML, however, reveals that from this point on more and more Au atoms are seen at the surface. In pronounced contrast to previous experimental interpretations[20,22] which agree that at 1-ML Au coverage the Au layer is almost completely buried below one Ag layer, we find at that coverage a

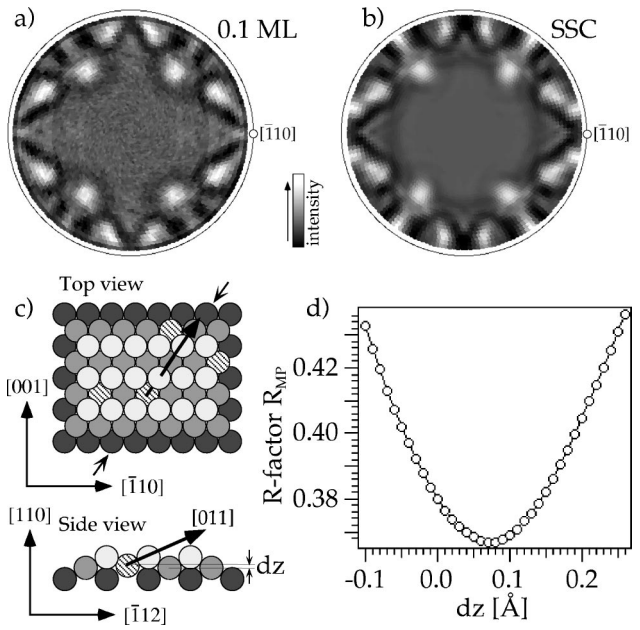

FIG. 4. Stereographic projection of experimental and calculated (SSC) Au $4f_{7/2}$ ($E_{kin}=1170.0$ eV) XPD patterns. (a) 0.1-ML-thick Au film. (b) SSC calculation using the atomic model of (c) and the best-fit parameters. (c) Top and side views ([$\bar{1}$12] azimuth) of the atomic model used to simulate (a). The small and large arrows indicate the side view plane and the [011] forward-scattering path, respectively. Au and Ag atoms are represented as hatched and filled circles (different shading indicates different layers). (d) *R*-factor curve obtained by comparing SSC calculations with the experimental Au $4f_{7/2}$ XPD pattern (a) as a function of the interlayer relaxation dz between the two outermost atomic layers in (c).

Au surface concentration of about 16%. Moreover, a nominal Au coverage of about 8 ML is required until no Ag atoms are detected by the ions. This finding is in good agreement with the MEIS study of Ref. 19 as well as the results of a surface core-level shift analysis.[22] The question arises of whether Ag atoms float on top of the growing Au overlayer, as proposed by the authors of Ref. 22, or if the Au growth proceeds via island formation. The latter is the case but, based on our LE-ISS data alone, it is not possible to answer this topographic question.

B. XPD experiments

Figure 4(a) displays the Au $4f_{7/2}$ XPD result obtained from a 0.1-ML-thick Au film. This experimental XPD pattern is very nicely reproduced by the single-scattering-cluster (SSC) calculation shown in Fig. 4(b), which has been done using the structural model [Fig. 4(c)] discussed in the following and uses the best-fit parameters of the *R*-factor analysis shown in Fig. 4(d).

The experiment [Fig. 4(a)] reveals twofold symmetry with prominent maxima at $\theta\approx 60°$ ($\langle 011\rangle$-type directions), $\theta\approx 73°$ ($\langle \bar{1}21\rangle$-type directions), $\theta\approx 77°$ ($\langle 013\rangle$-type directions) [see Fig. 1(b)]. All these peaks are caused by scattering of photoelectrons at atoms located in fcc sites one layer above the emitter. Surprisingly, no peaks appear at very grazing emission angles, i.e., as high as 88° off the surface normal. Moreover, no features originating from scattering at atoms located two or more layers above the photoemitter are present in the pattern.

Au-bilayer islands on top of the Ag(110) substrate—as proposed by Fenter and Gustafsson[19]—would account for the prominent maxima in the pattern of Fig. 4(a). However, in the case of small clusters on top of the substrate forward-focusing maxima for emission parallel to the surface are expected as well, i.e., along [$\bar{1}$10] or [001]. For instance, for the RT adsorption of Ag on Cu(001) such maxima have been reported.[32] In very good agreement with the STM study of Ref. 40, these data were interpreted in terms of 2D Ag clusters on top of the Cu(001) substrate.[32] Furthermore, for Au-bilayer islands one would expect a Au surface concentration n_{Au} of about 5% ($\frac{1}{2}\times 0.1$ ML) at this coverage, i.e., a Au surface concentration significantly larger than observed in our LE-ISS experiment (see Fig. 3).

Another conceivable structure is Au atoms substitutionally adsorbed in the top substrate layer with the replaced Ag atoms or subsequently adsorbed Au atoms located in the overlying hollow site. Again, it is the absence of forward-focusing maxima for grazing emission which excludes this possibility. As demonstrated for the 0.5-ML $c(2\times 2)$ Si/Cu(110) experiment, Si atoms substituted within the top layer are at the origin of the intense maxima observed at 88° off normal.[33] Moreover, the absence of features originating from scattering at atoms located two or more layers above the photoemitter excludes Au atoms to be buried deeper than one layer below the surface.

All in all, XPD demonstrates very directly that at Au coverages below 0.1 ML, most Au atoms are located within the second layer [Fig. 4(c)]. Furthermore, XPD indicates that the replaced Ag atoms diffuse away from the inverted Ag/Au areas. Otherwise, one would also observe maxima along $\langle 110\rangle$-, $\langle 010\rangle$-, and $\langle 112\rangle$-type directions [see Fig. 1(b)]. Note that diffusion of Ag atoms on the Ag(110) surface should not be a limiting factor, since Ag atoms are known to have a very high mobility on Ag(110) surfaces.[12,41]

In order to accurately determine atomic distances in the inverted Ag/Au model proposed above [see Fig. 4(c)], calculations have been performed using the SSC formalism.[8,28,31,36,42] The results of the calculations have been compared with the experiment by means of an *R* factor (R_{MP}) based on the space of multipole coefficients.[31–33] Besides the interlayer spacing z between the top Ag layer and the Au-Ag intermixed second layer, the effective mean free path λ_e of the Au $4f$ photoelectrons, and the effective inner potential V_o (Ref. 31) responsible for refraction at the surface potential step have been refined in the *R*-factor analysis. Figure 4(d) shows the *R*-factor value as a function of the interlayer relaxation dz.[43] The minimum of the curve corresponds to $dz=0.08\pm 0.1$ Å, which means that the interlayer distance between the two outermost atomic layers is relaxed by approximately 5.6%.

Our value for the contraction of the first-second layer spacing is somewhat smaller than the corresponding literature values for pure Ag(110), which vary from 7% to 10% as determined experimentally.[19,44–49] Our value is also smaller than the theoretically predicted 9% relaxation of an unreconstructed Au(110) surface.[50] As concerns the growth of Au on

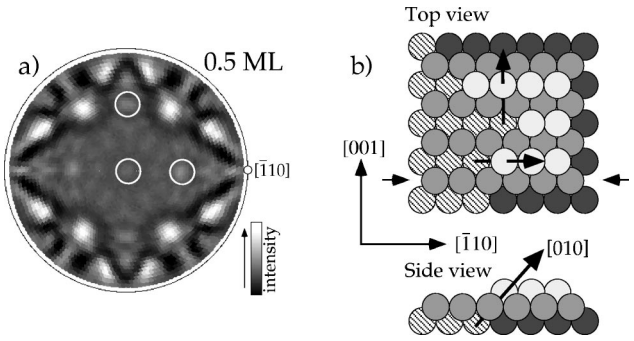

FIG. 5. Stereographic projection of the experimental Au $4f_{7/2}$ ($E_{kin}=1170.0$ eV) XPD pattern obtained from a 0.5-ML-thick Au film. The white circles mark the [112], [110], and [010] directions. (b) Top and side views ([$\bar{1}$10] azimuth) of the atomic model used to explain (a). The small and large arrows indicate the side view plane and the [010] and [112] forward scattering paths, respectively. Au and Ag atoms are represented as hatched and filled circles (different shading indicates different layers), respectively. 2D Ag islands (right-hand side) confined by inverted Ag/Au areas account for the maxima observed along ⟨010⟩- and ⟨122⟩-type directions (see text).

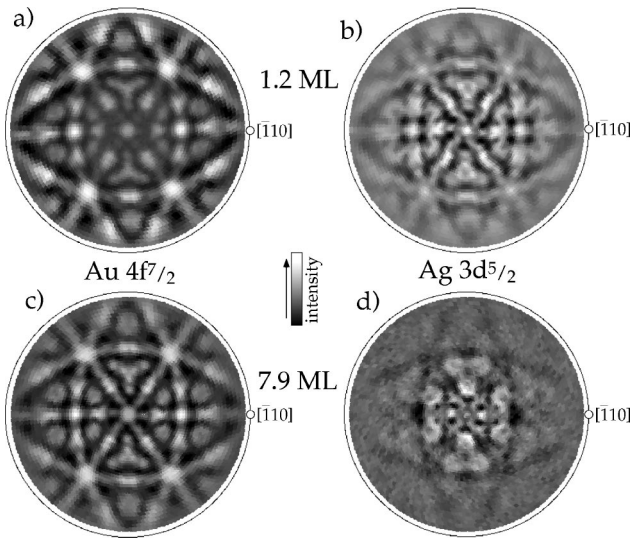

FIG. 6. Stereographic projections of the experimental Au $4f_{7/2}$ ($E_{kin}=1170.0$ eV) and Ag $3d_{5/2}$ ($E_{kin}=885.5$ eV) XPD patterns obtained from a 1.2-ML-thick Au film [Au $4f_{7/2}$ (a), Ag $3d_{5/2}$ (b)], and a 7.9-ML-thick Au film [Au $4f_{7/2}$ (c), Ag $3d_{5/2}$ (d)], respectively.

Ag(110), it compares well with the $6.3\pm0.3\%$ Au-Au relaxation found by Fenter and Gustafsson assuming a Au-bilayer growth model, thus a structure very different from our situation.[19] However, as was demonstrated by Rousset *et al.*[20] the MEIS data of Ref. 19 are also consistent with the inverted Ag/Au-layer model. Therefore, we would tend to say that the interlayer spacing is decreased upon the introduction of Au atoms into the second layer. Moreover, we find that Au atoms—as long as they are predominantly located in the second layer—are an excellent probe to monitor the first-to-second layer spacing of the inverted Ag/Au areas by means of XPD.

At the first view the Au $4f_{7/2}$ diffractogram taken from a 0.5-ML-thick Au film [Fig. 5(a)] is identical to the 0.1-ML experiment [Fig. 4(a)]. A closer look, however, reveals the presence of new very faint peaks along ⟨110⟩-, ⟨010⟩-, and ⟨112⟩-type directions [white circles in Fig. 5(a)]. All these maxima can be explained by scattering at atoms located two layers above the emitter. Rather surprising is the fact that the maxima along ⟨010⟩- and ⟨112⟩-type directions are more distinct than the normal-emission peak. It is surprising because on the one hand the atom-atom distance in a fcc crystal is shorter along the ⟨110⟩-type directions than along the ⟨010⟩- and ⟨112⟩-type directions. On the other hand it is known that the cross section for forward focusing decreases with increasing emitter-scatterer distance.[26] Therefore, for Au atoms buried two layers below the surface one would expect the normal emission peak to be more intense than the two other peaks.

In order to explain these unusual XPD patterns, we propose the following tentative model for the initial growth: Most of the deposited Au atoms penetrate to the second layer by an exchange-diffusion mechanism. The replaced Ag atoms diffuse away from the inverted Ag/Au areas, i.e., the inverted Ag/Au areas are not covered by diffusing Ag atoms (as shown by the low-coverage XPD), until they are trapped at the downhill side of step edges, or, until they meet another diffusing Ag atom giving rise to the nucleation of 2D Ag islands on the Ag(110) surface. With increasing Au coverage both the inverted Ag/Au areas as well as the 2D Ag islands expand, until they meet each other. Such a configuration is illustrated in the cluster of Fig. 5(b), where on the left- and right-hand sides an inverted Ag/Au area and an Ag island are sketched, respectively. As can be seen from the side view, forward-scattering paths exist along ⟨010⟩-, and ⟨112⟩-type directions (indicated by arrows), while there is no paths for normal emission. The very faint maxima observed in the [110] direction, finally, may be explained in terms of Au atoms falling on top of already inverted Ag/Au areas. This scenario also nicely fits our LE-ISS result (Fig. 3), which indicates a significant increase of the Au surface concentration above 0.5-ML Au coverage.

Figure 6 shows Au $4f_{7/2}$ and Ag $3d_{5/2}$ photoelectron distributions for two selected Au coverages above 0.8 ML, namely, 1.2 ML [Figs. 6(a) and 6(b)] and 7.9 ML [Figs. 6(c) and 6(d)]. A comparison with Fig. 1(b) shows that all observed maxima in the Au $4f_{7/2}$ diffractograms can be explained with the low-index directions and high-density planes of a fcc(110) crystal. Hence the Au growth follows the fcc(110) stacking sequence. The eight-leafed flower pattern[51] around the ⟨010⟩-type directions and the peaks along the ⟨111⟩-type directions observed above around 0.8-ML coverage are caused by scattering at atoms located five layers above the emitter. Assuming the formation of pure Au islands on the inverted Ag/Au areas, we conclude that the height of this Au islands is equal to three layers. Au surfaces are known to reconstruct in order to expose close-packed microfacets.[17] Therefore, spontaneous formation of 3D Au islands on inverted Ag/Au areas exposing three-row (111) microfacets, very similar to those in 1×3 MR-reconstructed surfaces, would account for this behavior. It is noteworthy that at least up to a Au coverage of 2.5 ML no additional peaks were identified in the XPD patterns, but that the eight-leafed flower pattern around the ⟨010⟩-type directions and the peaks along ⟨111⟩-type directions become more intense. This is indicative that below about 2.5-ML Au cov-

erage the average height of the Au islands remains constant, and that they essentially expand laterally.

Above 2.5-ML Au coverage, the (111)-plane intensity bands as well as the Y-shaped diffraction pattern centered around ⟨111⟩-type directions, which is typical for bulk emission from a fcc crystal at these electron energies,[51] become more intense, until, at 7.9-ML Au coverage [Fig. 6(c)] the pattern very closely resembles the Ag $3d_{5/2}$ diffractogram obtained from the clean Ag(110) surface [Fig. 1(a)]. After intermixing with Ag at the interface, Au grows three dimensionally on the Ag(110) surface, maintaining the same orientation as the underlying substrate.

As the Ag surface is covered with Au, those photoelectrons which travel longer inside the Au film are strongly damped. The intensities and anisotropies of the Ag $3d_{5/2}$ signal's are therefore low at grazing angles for Au coverages above 1 ML [Fig. 6(b)]. Moreover, at 7.9-ML coverage [Fig. 6(d)] the Ag $3d_{5/2}$ signal exhibits intensity minima along low-index directions and ''inverted'', low intensity Kikuchi bands[52] much like diffractograms taken from inelastically scattered electrons.[51] This indicates, in complete agreement with our LE-ISS result (Fig. 3), that above 7.9-ML coverage the Ag substrate is completely covered.

C. STM experiments

Figure 7 shows four representative STM experiments starting with the clean Ag(110) surface [Fig. 7(a)], being covered with 0.3-ML Au [Fig. 7(b)], 0.6-ML Au [Fig. 7(c)], and 1.9-ML Au [Fig. 7(d)]. This sequence of STM images illustrates the quick breakup of the surface into smaller terraces at Au submonolayer coverages.

A survey over many different scan areas shows that the clean Ag(110) surface is characterized by terraces separated by unevenly spaced monoatomic steps (1.45 Å high) mostly running along the $[\bar{1}10]$ direction, thus exposing energetically favorable (111) microfacets. In good agreement with previous STM studies,[21,53,54] we find that the terraces are usually several thousands Å long, while their widths vary from 50 Å up to about 2000 Å. Figure 7(a) shows an approximately 1000-Å large terrace bordered by two monoatomic steps running along $[\bar{1}10]$, with a half-unit-cell lateral shift of the close-packed rows of neighboring terraces in atomically resolved images.

The clean surface shows ''frizzy'' steps, with two consecutive images acquired from the same area presenting different images [Fig. 7(a)]. Frizziness of the steps was also observed for some other metal surfaces.[55–58] Although interpreted as dynamical effects, such as thermal diffusion or kink-creation processes at steps which are undersampled in time, the mechanism of such a motion is not yet understood. MD simulations using many-body tight-binding potentials indicate that the low activation barriers for both the Ag atom as well as the vacancy diffusion along $[\bar{1}10]$ steps may account for the frizziness of the steps.[41] On the other hand, a recent STM investigation[54] of the Ag(110) surface observed tip-assisted atom motion on Ag(110) even for large tunneling resistances ($R_t = 4$ GΩ) and, therefore, questions the previous interpretations of the frizziness of steps.

Figure 7(b) shows a representative STM picture for samples with 0.3-ML Au. Here one observes 2D islands

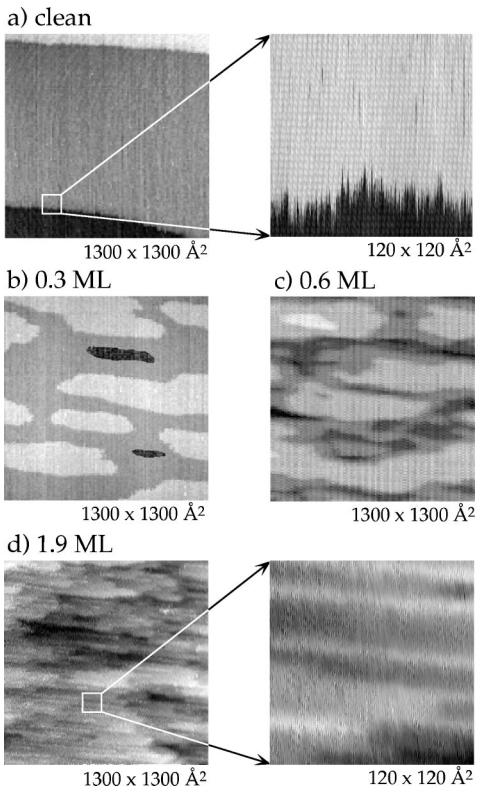

FIG. 7. STM topographs of (a) clean Ag(110), and (b) Ag(110) covered with 0.3-ML Au, (c) 0.6-ML Au, and (d) 1.9-ML Au, respectively. In all STM images the crystallographic $[\bar{1}10]$ direction is oriented along the horizontal direction to within $\pm 10°$. Linear background planes have been subtracted from the STM images, but further image processing was deemed unnecessary. The large scan area pictures are of size 1300×1300 Å^2, and the zoom in pictures of size 120×120 Å^2.

elongated along the $[\bar{1}10]$ direction on large terraces, while for regions where the steps are more closely spaced, the terraces are free of islands (not shown). Moreover, in some pictures we observe, in very good agreement with Ref. 21, the presence of holes elongated along $[\bar{1}10]$. Steps, especially those oriented along [001], develop sawtoothlike serrations (not shown). The growth of 2D fingerlike structures from the step edges reported by Rousset *et al.*[20] seems to correspond to these serrations. The slightly larger miscut angle of about 1° of the crystal used in the study of Ref. 20, compared to a miscut angle below 0.4° in the present study, has the consequence of a higher step density. This, in turn, may account for the absence of 2D islands in the STM study of Ref. 20 at a similar Au coverage. As indicated by LE-ISS (Fig. 3) and XPD (Figs. 4 and 5) measurements, respectively, at coverages below 0.5 ML most Au atoms are buried within the second substrate layer. Therefore, the islands and serrations mostly consist of replaced Ag atoms, while the Au atoms are buried below the original terraces. The rectangular shape of the islands reflects the anisotropy of the (110) substrate. Indeed, a MD calculation simulating the vapor deposition of Ag on Ag(110) shows that the anisotropic diffusion and sticking probabilities are responsible for the rectangular shape of the Ag islands observed in our experiment.[41]

Since the original Ag(110) surface does not exhibit holes, they are definitely the result of the Au deposition. The simul-

taneous positive (islands) and negative (holes) growth causes the surface to quickly break up into smaller terraces. This is illustrated by the STM image for 0.6-ML Au shown in Fig. 7(c). At this coverage the surface is characterized by holes and 1–2-layers-high islands including holes. Together with the low Au surface concentration revealed by LE-ISS measurements (see Fig. 3), this is indicative that the Au-Ag exchange mechanism is also active on the previously formed Ag islands. While the STM images below 0.5-ML Au coverage show frizzy step edges of both the islands and serrations, most step images now are stable. One explanation for this may be, as indicated by XPD (see Fig. 5), that the Ag islands are not allowed to overgrow inverted Ag/Au areas, confining the Ag mobility. An alternative argument is an increase of the bond strength due to the presence of Au atoms at or below the surface, as indicated by Nieminen's calculation of cohesive energies.[25] These arguments would also account for inhibiting tip-assisted atom motion.

Upon further Au deposition the surface grows increasingly rough due to numerous terraces elongated along $[\bar{1}10]$. In the case of a 1.9-ML-thick Au film [Fig. 7(d)], between 30% and 40% (see Fig. 3) of the surface consists of Au. Therefore, the rectangular shape of all observed islands reveals that the Au atoms also diffuse anisotropically on the surface. In particular, small scan area images reveal stripes running along $[\bar{1}10]$. Occasionally these stripes join together to form larger islands. Since we did not observe such stripes for submonolayer coverages we conclude that they consist of Au atoms. Three-dimensional, (1×3)-symmetric Au clusters similar to a generalized MR reconstruction would account for these stripes. Considering Nieminen's result[25] that the Au-Au bond is stronger than the Ag-Ag bond, the observation of 1D-like Au stripes rather than compact 2D islands can be understood from MD results simulating the vapor deposition of Ag on Ag(110),[41] if we assume an analogy between strengthening the bonding and reducing the temperature. In this simulation the various 1D stripes formed at low temperatures are found to become compact 2D aggregates at higher temperatures.

D. LEED experiments

Figure 8 displays four typical LEED experiments, starting with the Ag(110) surface being covered with 2.0 ML [Fig. 8(a)], 4.4 ML [Fig. 8(b)], 6.1 ML [Fig. 8(c)], and 7.5 ML [Fig. 8(d)], respectively. This sequence of LEED diagrams reveals the symmetry change on the surface upon Au deposition from 1×1, observed below 2.5 ML [Fig. 8(a)], to 1×2, detected above 7 ML [Fig. 8(d)]. The transition from 1×1 to 1×2 is characterized by LEED patterns exhibiting streaks along the [001]* direction of the reciprocal lattice as well as by poorly defined 1×3 spots at intermediate coverages [Figs. 8(b) and 8(c)]. The 1×3 phase, therefore, does not exist on the surface over large regions. Since the streaks are parallel to the [001]* direction, 1D disorder along the spatial [001] direction becomes evident.

It is interesting to compare the surface symmetry with the surface composition as determined by LE-ISS measurements (Fig. 3). In excellent agreement with the MEIS study of Ref. 19, we find that in the 1×1 phase as well as in the streaky 1×3 phase, a large fraction of the surface is composed of Ag

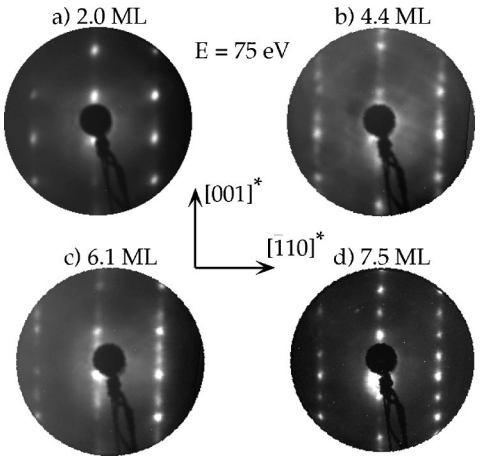

FIG. 8. Four selected LEED experiments ($E_{kin}=75$ eV), starting with the Ag(110) surface being covered with (a) 2.0 ML, (b) 4.4 ML, (c) 6.1 ML, and (d) 7.5 ML, respectively. In all LEED images the crystallographic $[\bar{1}10]$ direction is oriented along the horizontal direction to within $\pm5°$.

atoms. It is not until the 1×2 phase is formed that the surface is made exclusively of Au atoms. This is a clear sign that at this point Au completely covers the Ag substrate. Since wetting requires that the surface free energy of the film-substrate combination is lowered with respect to the clean surface,[4] one may argue that only the surface free energy of the 1×2 phase satisfies this condition, while the surface free energy of the 1×1 and 1×3 phase do not. Indeed, on the one hand Foiles, Baskes, and Daw,[23] using EAM potentials, found that the unreconstructed Au(110) surface has 24% more surface energy than the Ag(110) surface. On the other hand Nieminen's AEMF calculations revealed that the surface free energy of the 1×2 MR-reconstructed Au(110) surface is about 40% smaller than that of the Ag(110) surface.[25] However, due to the long range of interatomic potentials, Nieminen stated, in agreement with our experimental observation [Fig. 8(d)], that this argument is only valid for thick Au films. Therefore Nieminen's result may account for the surprisingly broad transition from the 1×1 to the 1×2 symmetry upon Au deposition. A further argument to explain this broad transition from the 1×1 to the 1×2 symmetry as well as arguments to explain the appearance of the 1×3 phase at intermediate Au coverages, is based on the study of Morgante *et al.*,[59] who investigated both the surface symmetries of $Ag_xAu_{1-x}(110)$ bulk alloys as well as that of the Ag/Au(110) growth system. On the one hand, for bulk alloys a 1×3 phase was found as soon as a critical Ag concentration was reached ($x\geqslant0.16\pm0.05$). On the other hand, RT deposition of ≈0.5-ML Ag on a 1×2 MR-reconstructed Au(110) surface induced broadening of the LEED spots along the [001]* direction. Upon annealing to 470 K the symmetry then converted to 1×3. All in all this indicates the tendency of the Au(110) surface to acquire a 1×3 symmetry upon the presence of small amounts of Ag at or near the surface. This, however, may very well account for our observations since Ag is present in the surface-layer up to 8 ML (see Fig. 3).

As revealed by STM (Fig. 7), the growth of Au on Ag(110) is characterized by the formation of holes and islands elongated along $[\bar{1}10]$, breaking up the surface into

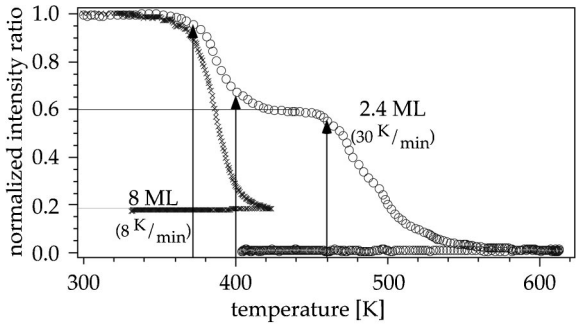

FIG. 9. Behavior of the XPS Au 4*d* to Ag 3*d* intensity ratios of a 2.4-ML-thick Au film (open circles) and a 8.0-ML-thick Au film (crosses) upon annealing with 30 and 8 K/min, respectively. The initial intensity ratios are normalized to unity. (The initial intensity ratio for 8 ML is greater than for 2.4 ML by a factor of ≈18.)

small terraces. For fcc(110) surfaces, various step configurations based on (111) microfacets such as 1×3 and (331) steps are known.[17,60–63] The formation of numerous small terraces along $[\bar{1}10]$, therefore, disturbs the periodicity along the spatial [001] direction, and causes the streaks along [001]* observed in our LEED patterns at intermediate coverages [Figs. 8(b) and 8(c)]. For further Au deposition more and more islands grow together and, consequently, the width of flat Au terraces increases. Locally this gives rise to well defined 1×3 phases observed as poorly formed 1×3 LEED diagrams [Fig. 8(c)]. As discussed above, the 1×3 phase seems to be stabilized by the presence of Ag near or at the surface.[59] For thick Au films, finally, the disappearance of the streaks in the LEED pattern reveals that the disorder along [001] is reduced, i.e., the roughness of the surface is decreased. Moreover, we end up with a well-defined 1×2 LEED diagram [Fig. 8(d)]. This is indicative of a smooth surface with 1×2 MR-reconstructed terraces extending over large regions. The smoothing of the previously very rough surface requires a large mass transfer. This, however, should not be a limiting factor in vapor deposition experiments.

Note, that the above discussed behavior can be compared to the two-phase transitions occurring on clean 1×2 MR-reconstructed Au(110) surfaces upon heating:[17,62,63] a 2D Ising transition at which the surface deconstructs, and a 3D roughening transition. STM studies indicate that the Ising transition of Au(110)(1×2) is due to antiphase domains developing during the 2D roughening of 1×3 steps (at ≈650 K). However, the MR configuration of interior terrace regions remains completely stable up to the 3D roughening temperature at around 700 K. The vapor deposition growth of Au on Ag(110) therefore may be considered as the reverse process.

E. Annealing experiments

As already mentioned in Sec. II, no significant dissolution of Au into the Ag bulk occurred at RT on the time scale of our experiments. This is consistent with the very small RT diffusion coefficient $D_{300\,\mathrm{K}}=5.5\times10^{-16}$ Å^2/sec of Au impurities in pure Ag derived from high-temperature (1000–1300 K) tracer diffusion data.[18]

Figure 9 displays the temperature dependence of the Au 4*d* to Ag 3*d* intensity ratio upon annealing of a 2.4-ML-thick Au film with 30 K/min (open circles), and a 8.0-ML-thick Au film with 8 K/min (crosses). Below 370 K the intensity ratios remain constant. For higher temperatures they reduce until an almost constant plateau is observed in the range from 400 up to 460 K. At higher temperatures a second intensity ratio decrease is observed, until no Au is detected with XPS at around 560 K. In the case of the 8-ML-thick Au film (crosses in Fig. 9), the heating was stopped at 430 K, i.e., in the plateau regime of temperatures. During the subsequent cooling the intensity ratio remained constant. Note that the intensity ratios of the other Au films exhibit a similar temperature dependence.

The diffusion coefficient at 460 K ($D_{460\,\mathrm{K}}=9.5\times10^{-4}$ Å^2/sec) is 12 orders of magnitude larger than at RT. As estimated from Fick's second law, bulk diffusion should become significant on the time scale of our experiment above 460 K.[64] Therefore, we attribute the second intensity ratio decrease to diffusion of the Au atoms into the Ag bulk, while the first one seems to be characteristic of a surface processes, e.g., surface energy driven diffusion of Ag atoms to the surface. Note that diffusion coefficients in general are expected to be substantially higher in the near-surface region because the force constants are reduced relative to the bulk, and the surface acts as an efficient source of vacancies favoring exchange-diffusion mechanisms.[59]

In the special case of the 2.4-ML-thick Au film at the plateau, the intensity ratio corresponds to about 60% of the initial value. According to our growth model (see below) the initial structure of the 2.4-ML-thick Au film includes about 10% pure Ag-bulk regions, 40% inverted Ag/Au areas, and the remaining 50% consist of in average three-layer-high Au islands on inverted Ag/Au areas. Assuming the structure of the annealed sample at the plateau to be 2.4 Au layers buried below one Ag layer, a reduction of the intensity ratio to 73% of the initial value is expected.[65] In an analogous manner we find that the intensity ratio of the 8-ML-thick Au film should reduce to 31% of its initial value (experimental value 19%, Fig. 9). Even though this concept underestimates the experimental intensity ratio reductions, it supports the assumption that the first intensity ratio reduction is caused by a surface-driven process.

IV. GROWTH MODEL

In this section we first propose a model for the RT growth of Au on Ag(110) which is based on our experimental findings. Then we will establish the coverage dependence of the different structures involved in that model. Finally, the model will be compared to both thermodynamic equilibrium predictions[12,23–25] and to results obtained from MD simulations.[12]

Figure 10 illustrates the growth model displaying the starting Ag(110) surface [Fig. 10(a)], covered with a very thin Au film (<0.5-ML) [Fig. 10(b)] and after deposition of more than 0.5-ML Au [Fig. 10(c)]. The Ag atoms are drawn as filled circles, with different shadings indicating different layers. Note that in Figs. 10(b) and 10(c) the replaced Ag atoms are drawn in shading corresponding to their original positions in Fig. 10(a). The Au atoms are sketched as hatched circles. The arrows indicate the positions of steps.

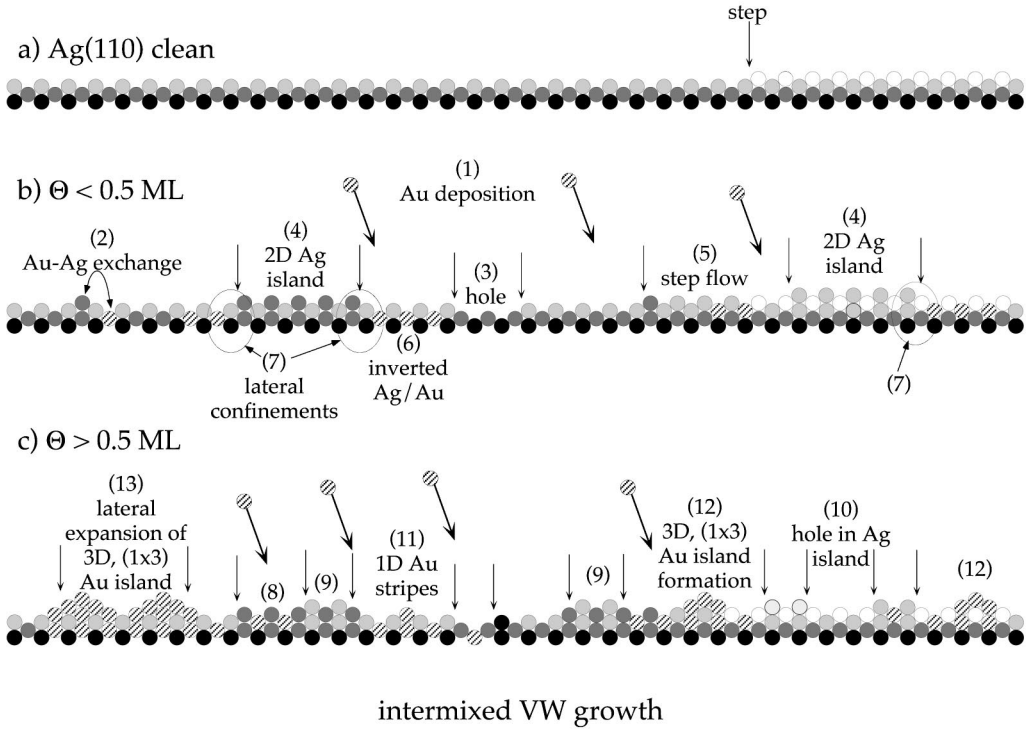

FIG. 10. Side views ([$\bar{1}$12] azimuth) of the atomic configurations developing upon the Au deposition illustrating the intermixed VW growth model proposed in Sec. IV. (a) Clean Ag(110) surface. (b) Very low Au coverages (below 0.5 ML). (c) Au coverages above 0.5 ML. Au and Ag atoms are represented as hatched and filled circles (different shading indicates different layers). Step positions are indicated by arrows. The quick breakup of the surface into smaller terraces becomes evident in this model.

The numbers design the most important steps and results of the model and are also given in bold style in the text below.

The clean, unreconstructed Ag(110) surface is characterized by large terraces which are separated by monoatomic steps [Fig. 10(a)]. Upon vapor deposition of Au on the clean, unreconstructed Ag(110) surface, the Au atoms are randomly distributed on the surface (1) [Fig. 10(b)]. Au atoms falling on the bare Ag bulk become buried one layer below the surface by a Au-Ag exchange mechanism (2) [as demonstrated by XPD (Figs. 4 and 5) and LE-ISS (Fig. 3)]. It is a simple process for a deposited Au atom to exchange with a Ag atom in the top layer. Indeed, cross-channel exchange mobility on (110) faces of fcc transition metals has been observed in many experiments and simulations.[41,66,67] However, for the Au atom to dig further into the second layer, it would be a difficult process involving a large energy barrier. This barrier would be that for interstitial formation, which is known to be quite large for fcc noble metals, making the process very unlikely at RT.

For Au atoms to become buried within the second substrate layer an alternate path of much lower resistance was proposed by Hirschorn *et al.*[21]: In a first step, a Au adatom exchanges its place with a Ag atom in the top layer. Subsequently a Ag atom in the first layer next to the Au is ejected to create a vacancy. The vacancy becomes filled by a Ag atom in the second layer below the Au atom, and the Au atom moves in to fill the position in the second layer (see Fig. 5 of Ref. 21). The net result is a vacancy formed on the surface with two Ag atoms ejected which can either diffuse to form 2D Ag islands, diffuse to nearby step edges, or back fill the surface vacancy.

In the mechanism proposed by Hirschorn *et al.*, no interstitials are ever formed during the entire process, and this requirement of avoiding atomic compression necessitates the movement of a Ag atom in the first layer to above the surface (vacancy creation). The important question here is the energy barrier for vacancy creation. However, since the Ag(110) can easily be made to undergo a MR reconstruction with minor surface perturbations,[68] the energy barrier for vacancy creation is expected to be quite low. In fact, one side of the vacancy is occupied by a Au atom, and Au does favor the MR reconstruction.[17,60–63]

In Fig. 10(b) the most important topographic features as expected from Hirschorn *et al.*'s Au-Ag exchange mechanism are sketched for coverages below 0.5 ML: Once the vacancies are formed, they can diffuse just like adatoms[41] and agglomerate to form a vacancy cluster (hole) (3).[69] The ejected Ag atoms diffuse to nucleate 2D Ag islands (4) on terraces or are at the origin of step flow (5) when they reach step edges. Note that the Ag atoms diffuse away from inverted Ag/Au areas (6) (as indicated by XPD, Figs. 4 and 5), and therefore the 2D Ag islands nucleate on the bare Ag bulk. Due to the anisotropic diffusion barriers for Ag atoms and vacancies, and anisotropic probabilities for atoms to stick on island edges,[41] the Ag islands and holes are elongated along [$\bar{1}$10]. Indeed, elongated-shaped islands and holes are observed with STM at low coverages [Fig. 7(b)].

For subsequently deposited Au atoms falling on bare Ag-bulk areas or 2D Ag islands the above-discussed Au-Ag exchange mechanism is going on. Therefore, the 2D islands as well as the inverted Ag/Au areas expand laterally, until they

meet each other. However, as already mentioned above, XPD indicates that the 2D Ag islands do not overgrow the inverted Ag/Au areas (Figs. 4 and 5). The reduction of the step mobility observed with STM, therefore, may be caused by the confinement of the lateral expansion of both features (7) [Fig. 10(b)]. As sketched in Fig. 10(c), the Au-Ag exchange mechanism on previously formed 2D Ag islands yields inverted Ag/Au areas with the Au layer located in the original top layer (8), as well as vacancies within the islands and Ag atoms on the islands. These vacancies and Ag atoms can either diffuse to form 2D Ag islands on the islands (9) or holes within the islands (10), respectively, in good agreement with our STM results [Fig. 7(c)].

Au atoms falling on already inverted Ag/Au areas also diffuse anisotropically on the surface. Due to the strong Au-Au bond they are, however, less mobile than the Ag atoms. (Note that Au atoms of the inverted Ag/Au configuration are nearest neighbors for diffusing Au atoms when located in a hollow site). Nevertheless, if they reach the border of inverted Ag/Au areas they become buried in the second layer by the already discussed Au-Ag exchange mechanism. Otherwise, due to the strong Au-Au bond,[25] they start to form 1D Au stripes on inverted Ag/Au areas (11). This stripes are very similar to the Ag stripes predicted in the MD simulation of low-temperature vapor deposition of Ag on Ag(110).[41] In order to reduce the surface energy,[25] and driven by the tendency of Au to form close-packed microfacets,[17,70] the Au stripes congregate and start to form 3D, (1×3)-symmetric Au islands (12). This is consistent with our STM data (Fig. 7) as well as with our XPD results (Fig. 6) indicating that three layer high Au islands start to be present already at 0.8-ML Au coverage.

Au atoms deposited on already existing Au islands remain on the Au islands due to the strong Au-Au bond[25] as well as due to surface energetics. As a consequence the 3D, (1×3)-symmetric Au islands laterally expand upon further Au deposition (13). This is indeed indicated by XPD (Fig. 6) and LEED, where we observe a poorly formed streaky 1×3 LEED pattern in the range from 2.5 up to 7.0 ML (Fig. 8). The streaks are clearly related to the disorder in the spatial [001] direction caused by the numerous small terraces and Au islands elongated along $[\bar{1}10]$. With further Au deposition the disorder along [001] reduces, i.e., the roughness of the surface is decreased, until 1×2 MR-reconstructed terraces extend over regions as large as to yield a well-defined 1×2 LEED pattern at around 8-ML Au coverage. At this point the surface is completely covered with Au (see Fig. 3).

All in all our model states that the growth is characterized by an Au-Ag exchange yielding an inverted Ag/Au layer, followed by a 3D pileup of Au on top of such inverted Ag/Au areas. Note that locally the Au island formation starts, while other areas of the surface still are terminated with a pure Ag(110) surface or an inverted Ag/Au configuration. This is in contrast to Rousset *et al.*'s intermixed SK growth model,[20] which claims that 3D Au islands growth starts only after the formation of one complete inverted Ag/Au layer. Following their nomenclature we assign our growth model as an intermixed VW growth.

Figure 11 shows a schematic drawing of the three different surface structures which, according to the intermixed VW growth model, develop on the surface with increasing

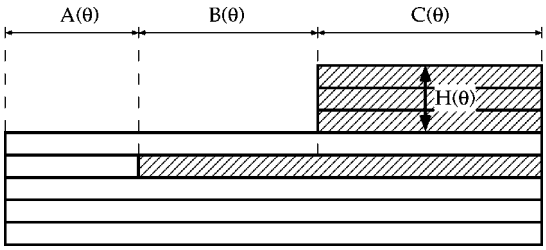

FIG. 11. Schematic drawing of the three different surface structures existing on the surface in the context of the intermixed VW growth model. These structures have been used to fit the LE-ISS data (see Fig. 3) as described in the text. Ag and Au layers are drawn as open and hatched rectangles, respectively: bare Ag-bulk areas $A(\Theta)$, inverted Ag/Au areas $B(\Theta)$, and 3D Au islands on inverted Ag/Au areas $C(\Theta)$. The average number of layers $H(\Theta)$ of the 3D Au islands on inverted Ag/Au areas is indicated by the double-headed arrow.

coverage Θ: $A(\Theta)$ denominates bare Ag-bulk areas, $B(\Theta)$ is used for the inverted Ag/Au areas, and the 3D Au islands on the inverted Ag/Au areas are assigned to $C(\Theta)$. $A(\Theta)$, $B(\Theta)$, and $C(\Theta)$ take values ranging from 0 to 1. In the following their coverage dependence will be established respecting the conditions given by our growth model. (1) Au atoms falling on bare Ag-bulk regions result in a reduction of $A(\Theta)$, and to a corresponding increase of $B(\Theta)$. (2) Au deposited on inverted Ag/Au areas results in a decrease of $B(\Theta)$ and in a corresponding increase of $C(\Theta)$. (3) For Au falling on Au islands, finally, $C(\Theta)$ remains unchanged, but the average number of layers $H(\Theta)$ of the pure 3D Au islands on the inverted Ag/Au areas increases. Assuming that during an infinitesimal coverage increase $d\Theta$ the probability for a Au atom to be deposited on one of the three different structures is proportional to the area of that structure, it follows that

$$A(\Theta)=A(\Theta-d\Theta)-d\Theta\cdot A(\Theta-d\Theta) - e(\Theta)\cdot d\Theta\cdot B(\Theta-d\Theta), \tag{3}$$

$$B(\Theta)=B(\Theta-d\Theta)+d\Theta\cdot A(\Theta-d\Theta) + e(\Theta)\cdot d\Theta\cdot B(\Theta-d\Theta) - k(\Theta)\cdot d\Theta\cdot B(\Theta-d\Theta), \tag{4}$$

$$C(\Theta)=C(\Theta-d\Theta)+k(\Theta)\cdot d\Theta\cdot B(\Theta-d\Theta). \tag{5}$$

The parameter $e(\Theta)$ accounts for the possibility that a Au atom deposited on an inverted Ag/Au area can reach the border of that area, and by Au-Ag exchange reduce and increase areas $A(\Theta)$ and $B(\Theta)$, respectively. Parameter $k(\Theta)$, on the other hand, accounts for the tendency of Au to congregate and to form 3D islands instead of growing layer by layer. Calculating the total number of ML's present on the areas B and C [$H\cdot C+(B+C)\cdot 1)=\Theta$, see Fig. 11], $H(\Theta)$ can be calculated as follows:

$$H(\Theta)=\frac{\Theta-[B(\Theta)+C(\Theta)]}{C(\Theta)}. \quad (6)$$

As can be seen from Fig. 11, $C(\Theta)$ corresponds to the Au surface concentration n_{Au}, i.e., a quantity which was measured with LE-ISS (see Fig. 3). Thus, Eqs. (3)–(5) can be used to fit the LE-ISS data (open diamonds in Figs. 3). For simplicity $e(\Theta)$ was set to zero, and the remaining fitting parameter $k(\Theta)$ was assumed to be independent of the coverage Θ. In the present case the best fit [solid curve in Fig. 3] was achieved with $k=0.52$. The dotted curve and the hairline curve in Fig. 3 show the evolution of bare Ag areas and inverted Ag/Au areas, respectively, for this best fit.

At low coverages $H(\Theta)$ is overestimated compared to our experimental results. This is caused by the neglection of the possibility for Au atoms diffusing on inverted Ag/Au areas to reach bare Ag-bulk areas. At low coverages, i.e., for small inverted Ag/Au areas this process may be important. Furthermore, $H(\Theta)$ depends very sensitively on $k(\Theta)$. Our assumption that $k(\Theta)$ is constant for all coverages does not hold for submonolayer coverages. Indeed, the exclusive observation of 2D islands at 0.1 ML corresponds to $k=1$. However, it is noteworthy that in the range from about 0.8 ML up to 3.0 ML, C(Θ) increases from 11% to 62% (see Fig. 3), while $H(\Theta)$ only increases from 2.2 to 3.3 layers. This is in good agreement with our experimental XPD and LEED results, indicating that in this regime of coverages 3D, (1×3)-symmetric Au islands laterally expand. As an estimate for k we can imagine one flat Au layer rearranged into 3D, (1×3)-symmetric Au islands. The result is a half-covered surface, i.e., $k=0.5$, in very good agreement with our optimal k value of 0.52.

It is interesting to compare the intermixed VW growth model to the structures predicted by theoretical studies.[12,23–25] According to our model, Au atoms deposited on bare Ag-bulk areas or on previously formed 2D Ag islands become buried one layer below the surface. The formation of inverted Ag/Au areas on the surface fits nicely thermodynamic equilibrium predictions based on the SEAM,[12] DFT,[24] and AEMF methods,[25] respectively. These studies agree in that the most favorable configuration for one Au layer is to burrow one layer below the surface. At 1-ML Au coverage, however, the structure of the surface extracted from our model (36% pure Ag-bulk regions, 48% inverted Ag/Au areas, and 16% in average 2.8-layer-high Au islands on inverted Ag/Au areas) deviates significantly from the simple inverted Ag/Au-layer picture preferred by equilibrium thermodynamics (crosses in Fig. 3). This is indicative for kinetic considerations to play an important role in the Au/Ag(110) growth system.

As discussed above, the Au-Ag exchange mechanism proposed by Hirschorn *et al.*[21] should not be a limiting factor of the growth process. Furthermore, Ag atoms and vacancies are known to be very mobile on Ag(110).[41] Therefore, Ag atoms and vacancies resulting from the Au-Ag exchange mechanism are expected to arrange themselves in an energetically favorable configuration as well. Indeed, as indicted by XPD (Figs. 4 and 5), ejected Ag atoms seem to diffuse away from inverted Ag/Au areas, avoiding the formation of areas with Au buried below two Ag layers. According to DFT (Ref. 24) and SEAM,[12] structures including Au atoms buried below two Ag layers are not favorable. This is also consistent with our result that 2D Ag islands are not allowed to overgrow inverted Ag/Au areas.

Au atoms deposited on inverted Ag/Au areas, however, are much less mobile. This can be understood by taking into account, first, the strong Au–Au bond,[25] and, second, the open geometry of fcc(110) surfaces. Indeed, the side view along the $[\bar{1}10]$ azimuth (see Figs. 2, 4, and 10) reveals that one of the five nearest neighbors of a Au atom located in a hollow site of an inverted Ag/Au area is a Au atom. As a consequence of the reduced mobility only part of the diffusing Au atoms reach the border of the inverted Ag/Au area. There they become buried within the second layer acquiring an energetically favorable position. The rest of the diffusing Au atoms, which cannot undergo the Au-Ag exchange, consequently seek to build other energetically favorable structures on the inverted Ag/Au areas. In our growth model we state that due to the strong Au-Au bond, 1D Au stripes start to form. Then, in order to reduce the surface energy, the Au stripes congregate to form 3D, (1×3)-symmetric Au islands which expand laterally upon further Au deposition. This scenario fits nicely Nieminen's AEMF calculations[25] which in the range of 3–6 ML predict the formation of 3D, (1×3)-symmetric Au clusters similar to a generalized MR reconstruction on a completely inverted Ag/Au layer. Moreover, in excellent agreement with our experimental results, Nieminen finds that only thick 1×2 MR-reconstructed Au films satisfies the wetting conditions.

Further indications for the topology of the Au films to be determined by the limitation of the Au mobility is given by the comparison of our intermixed VW growth model with Haftel *et al.*'s MD simulations.[12] In very good agreement with our results, these simulations find that the most probable dynamic processes are atomic replacement of Au atoms with substrate Ag, and surface hopping of Ag atoms along the $[\bar{1}10]$ channels. Furthermore, Au atoms falling on top of Au atoms are predicted to be relatively immobile. The Au-Ag exchange mechanism ''preferred'' by MD simulations, however, is significantly different from our experimental findings in that the Au adatoms exchange with Ag atoms in the top layer, rather than with second layer Ag atoms. In Haftel *et al.*'s model,[12] most of the Au atoms are uncovered at low coverages ($\leqslant$0.5 ML) due to the high mobility of the substituted Ag atoms on Ag(110). This yields a Au surface concentration (filled triangles in Fig. 3) which is significantly larger (by a factor of 8) than our experimental findings (open diamonds). Therefore, together with STM (observation of holes, Fig. 7 and Ref. 21) and our XPD results (Fig. 4), Haftel *et al.*'s Au-Ag exchange mechanism can be ruled out. At higher coverages, however, MD simulations agree with our results. Substituted Ag atoms start to cover Au atoms resulting in inverted Ag/Au areas with about 70% of the Au atoms resident below the complete adlayer at 1-ML coverage. Increasingly, incident Au atoms then stick on inverted Ag/Au areas until at 3.0-ML 3D (1×3)-symmetric Au ridges are evident. In good agreement with our model, it is the reduced Au mobility on inverted Ag/Au areas, together with the lowering of the surface energy, which is at the origin of the 3D Au island formation.

V. CONCLUSIONS

All in all we find that the initial RT growth of Au on Ag(110) follows an intermixed VW growth mode. This model is characterized by a Au-Ag exchange mechanism ending up with the Au atom buried within the second layer, a vacancy formed on the surface and two ejected Ag atoms. The anisotropic diffusion of both the vacancies and ejected Ag atoms results in step flow, 2D Ag islands, and holes elongated along $[\bar{1}10]$. Our results indicate that these rectangular Ag islands are not allowed to overgrow inverted Ag/Au areas. The formation of 2D Ag islands and holes causes the surface to break up quickly into smaller terraces at submonolayer coverages. Due to the strong Au-Au bond,[25] Au atoms deposited on inverted Ag/Au areas are much less mobile than Ag atoms. (Note that Au atoms of the inverted Ag/Au configuration are nearest neighbors of a diffusing Au atom when located in a hollow site.) Therefore, an increasing part of diffusing Au atoms will not reach the border of the inverted Ag/Au area, where they would become buried in the energetically favorable second-layer positions.[12,23–25] It is this kinetic limitation which hinders the formation of one complete inverted Ag/Au layer. Due to the strong Au-Au bond, Au atoms diffusing on inverted Ag/Au areas start to form 1D Au stripes, and in order to reduce the surface energy such stripes congregate resulting in 3D, (1×3)-symmetric Au islands already at submonolayer coverages. Upon further deposition the Au islands then expand both in vertical and horizontal directions, until Ag is completely covered at more than 8 ML. At this point the surface consists of 1×2 MR-reconstructed terraces extending over regions as large as to yield a sharp 1×2 LEED pattern. This result indicates that only 1×2 MR-reconstructed Au(110) surfaces satisfy the wetting conditions as predicted by Nieminen.[25] The resulting interface is intermixed over several layers. This nicely fits Niklasson, Abrikosov, and Johansson's prediction using the IFME's in that the Ag-Au interface is not sharp at RT.[11] However, our results demonstrate that the Au films do not dissolute into the Ag bulk at RT. We find that dissolution into the bulk starts at around 460 K, while interdiffusion at the surface is already evident at 370 K.

ACKNOWLEDGMENTS

We profited from stimulating discussions with A. Schneuwly and P. Gröning. Skillful technical assistance was provided by F. Bourqui, Ch. Neururer, E. Mooser, and O. Raetzo. This project was supported by the Fonds National Suisse pour la Recherche Scientifique.

*Electronic address: Josef.Hayoz@unifr.ch

[1] J. A. Venables, G. D. T. Spiller, and M. Hanbücken, Rep. Prog. Phys. **47**, 399 (1984).

[2] P. Grünberger, R. Schreiber, Y. Pang, M. B. Brodsky, and H. Sowers, Phys. Rev. Lett. **57**, 2442 (1986).

[3] M. N. Baibich, J. M. Broto, A. Fert, F. Nguyen van Dau, F. Petroff, P. Etienne, G. Creuzet, A. Friedrich, and J. Chazelas, Phys. Rev. Lett. **61**, 2472 (1988).

[4] E. Bauer, Z. Kristallogr. **110**, 372 (1958).

[5] E. Bauer and J. H. v.d. Merwe, Phys. Rev. B **33**, 3657 (1986).

[6] D. Naumović, P. Aebi, A. Stuck, P. Schwaller, J. Osterwalder, and L. Schlapbach, Surf. Sci. **307–309**, 483 (1994).

[7] D. Naumović, J. Osterwalder, A. Stuck, P. Aebi, and L. Schlapbach, Surf. Sci. **287/288**, 950 (1993).

[8] A. Stuck, R. Fasel, J. Osterwalder, and L. Schlapbach, Surf. Rev. Lett. **1**, 229 (1994).

[9] L. P. Nielsen, F. Besenbacher, I. Stensgaard, and E. Lægsgaard, Phys. Rev. Lett. **71**, 754 (1993).

[10] J. Tersoff, Phys. Rev. Lett. **74**, 434 (1995).

[11] A. M. N. Niklasson, I. A. Abrikosov, and B. Johansson, Phys. Rev. B **58**, 3613 (1998).

[12] M. I. Haftel, M. Rosen, T. Franklin, and M. Hettermann, Phys. Rev. Lett. **72**, 1858 (1994); M. I. Haftel and M. Rosen, Phys. Rev. B **51**, 4426 (1995).

[13] A. Schneuwly, Ph.D. thesis, University of Fribourg, Switzerland, 1998; A. Schneuwly, P. Gröning, L. Schlapbach, and V. P. Jaecklin, J. Electron. Mater. **27**, 990 (1998); A. Schneuwly, P. Gröning, L. Schlapbach, and G. Müller, *ibid.* **27**, 1254 (1998).

[14] J. Hayoz, Th. Pillo, D. Naumović, P. Aebi, and L. Schlapbach, Surf. Sci. (to be published).

[15] Electrum is one of the oldest alloys known to mankind, and was already prized by the ancient Egyptians.

[16] J. White, R. Orr, and R. Hultgren, Acta Metall. **5**, 747 (1957).

[17] R. Koch, M. Borbonus, O. Haase, and K. H. Rieder, Appl. Phys. A: Solids Surf. **55**, 417 (1992), and references therein.

[18] W. C. Mallard, A. B. Gardner, R. F. Bass, and L. M. Slifkin, Phys. Rev. **129**, 617 (1963).

[19] P. Fenter and T. Gustafsson, Phys. Rev. Lett. **64**, 1142 (1990); Phys. Rev. B **43**, 12 195 (1991).

[20] S. Rousset, S. Chiang, D. E. Fowler, and D. D. Chambliss, Phys. Rev. Lett. **69**, 3200 (1992); Surf. Sci. **287/288**, 941 (1993); J. Vac. Sci. Technol. B **12**, 1747 (1994).

[21] E. S. Hirschorn, D. S. Lin, E. D. Hansen, and T.-C. Chiang, Surf. Sci. **323**, L299 (1995).

[22] E. S. Hirschorn, T. Miller, M. Sieger, and T.-C. Chiang, Surf. Sci. Lett. **295**, L1045 (1993).

[23] S. M. Foiles, M. I. Baskes, and M. S. Daw, Phys. Rev. B **33**, 7983 (1986).

[24] C. T. Chan, K. P. Bohnen, and K. M. Ho, Phys. Rev. Lett. **69**, 1672 (1992).

[25] J. A. Nieminen, Surf. Sci. **344**, L1213 (1995).

[26] C. S. Fadly, in *Synchrotron Radiation Research: Advances in Surface Science*, edited by R. Z. Bachrach (Plenum, New York, 1990), Vol. 1.

[27] J. Osterwalder, P. Aebi, R. Fasel, D. Naumović, P. Schwaller, T. Kreutz, L. Schlapbach, T. Abukawa, and S. Kono, Surf. Sci. **331–333**, 1002 (1995).

[28] R. Fasel, P. Aebi, R. G. Agostino, D. Naumović, J. Osterwalder, A. Santaniello, and L. Schlapbach, Phys. Rev. Lett. **76**, 4733 (1996).

[29] P. Aebi, R. Fasel, D. Naumović, J. Hayoz, Th. Pillo, M. Bovet, R. G. Agostino, L. Patthey, L. Schlapbach, F. G. Gil, H. Berger, T. J. Kreutz, and J. Osterwalder, Surf. Sci. **402**, 614 (1998).

[30] J. Hayoz, S. Sarbach, Th. Pillo, D. Naumović, P. Aebi, and L. Schlapbach, Phys. Rev. B **58**, R4270 (1998).

[31] R. Fasel, P. Aebi, J. Osterwalder, and L. Schlapbach, Surf. Sci. **331–333**, 80 (1995); Phys. Rev. B **52**, R2313 (1995); R. Fasel, P. Aebi, J. Osterwalder, L. Schlapbach, R. G. Agostino, and G.

Chairello, *ibid.* **50**, 14 516 (1994).
[32] J. Hayoz, D. Naumović, R. Fasel, P. Aebi, and L. Schlapbach, Surf. Sci. **373**, 153 (1997).
[33] J. A. Martin-Gago, R. Fasel, J. Hayoz, R. G. Agostino, D. Naumović, P. Aebi, and L. Schlapbach, Phys. Rev. B **55**, 12 896 (1997).
[34] H. Niehus, W. Heiland, and E. Taglauer, Surf. Sci. Rep. **17**, 213 (1993).
[35] E. Taglauer and W. Heiland, Appl. Phys. (Berlin) **9**, 261 (1976).
[36] J. Osterwalder, T. Greber, A. Stuck, and L. Schlapbach, Phys. Rev. B **44**, 13 764 (1991).
[37] Danish Micro Engineering, Herlev, Denmark.
[38] M. P.. Seah and W. A. Dench, Surf. Interface Anal. **1**, 2 (1979).
[39] The $P_{\mathrm{Au}}/P_{\mathrm{Ag}}$ ratio was estimated by measuring the scattered ion intensities I_{Ag} from a clean Ag(111) single crystal, and I_{Au} from a clean Au(111) single crystal. Since the ion incidence direction was selected to be parallel to same crystal directions for both surfaces, the number of scattering centers on the Ag(111) surface, n_{Ag}, and on the Au(111) surface, n_{Au}, respectively, are equal. For both crystals the measurements were repeated several times by alternating between the Ag(111) and Au(111) crystal, without switching off the ion gun. Consequently, the primary ion intensity I_o can be considered constant during the experiment, and to be identical for the two surfaces. Under these experimental conditions the $P_{\mathrm{Au}}/P_{\mathrm{Ag}}$ ratio finally depends only on the measured $I_{\mathrm{Au}}/I_{\mathrm{Ag}}$ ratio and on the calculated $d\sigma_{\mathrm{Au}}/d\sigma_{\mathrm{Ag}}$ ratio. We find a $P_{\mathrm{Au}}/P_{\mathrm{Ag}}$ ratio of 0.95.
[40] P. T. Sprunger, E. Lægsgaard, and F. Besenbacher, Phys. Rev. B **54**, 8163 (1997).
[41] F. Hontinfinde, R. Ferrando, and A. C. Levi, Surf. Sci. **366**, 306 (1996); R. Ferrando, F. Hontinfinde, and A. C. Levi, *ibid.* **402–404**, 286 (1998).
[42] D. J. Friedman and C. S. Fadley, J. Electron Spectrosc. Relat. Phenom. **51**, 689 (1990).
[43] In all the calculations shown here, the optimum values of 13.7 eV for V_o and 5.0 Å for λ_e have been used.
[44] E. Holub-Krappe, K. Horn, J. W. M. Frenken, R. L. Krans, and J. F. van der Veen, Surf. Sci. **188**, 335 (1987).
[45] Y. Kuk and L. C. Feldman, Phys. Rev. Lett. **30**, 5811 (1984).
[46] C. L. Fu and K. M. Ho, Phys. Rev. Lett. **63**, 1617 (1989).
[47] M. Lindroos, C. J. Barnes, M. Valden, and D. A. King, Surf. Sci. **218**, 269 (1989).
[48] G. Bracco, M. Canepa, P. Cantini, F. Fossa, L. Mattera, S. Terreni, and D. Truffelli, Surf. Sci. **269/270**, 61 (1992).
[49] B. W. Busch and T. Gustafsson, Surf. Sci. **407**, 7 (1998).
[50] K.-M. Ho and K. P. Bohnen, Europhys. Lett. **4**, 345 (1987).
[51] D. Naumović, A. Stuck, T. Greber, J. Osterwalder, and L. Schlapbach, Phys. Rev. B **47**, 7462 (1993).
[52] R. Trehan, J. Osterwalder, and C. S. Fadley, J. Electron Spectrosc. Relat. Phenom. **42**, 187 (1987).
[53] W. W. Pai, N. C. Bartelt, and J. E. Reutt-Robey, Phys. Rev. B **53**, 15 991 (1996).
[54] J. Li, R. Berndt, and W. D. Schneider, Phys. Rev. Lett. **76**, 1888 (1996).
[55] J. W. M. Frenken, R. J. Hamers, and J. E. Demuth, J. Vac. Sci. Technol. A **8**, 293 (1990).
[56] J. Frohn, M. Giesen, M. Poensgen, J. F. Wolf, and H. Ibach, Phys. Rev. Lett. **67**, 3543 (1991); M. Poensgen, J. F. Wolf, J. Frohn, M. Giesen, and H. Ibach, Surf. Sci. **274**, 430 (1992).
[57] S. Speller, W. Heiland, A. Biedermann, E. Platzgummer, C. Nagl, M. Schmid, and P. Varga, Surf. Sci. **331**, 1056 (1995).
[58] M. Dietterle, T. Will, and D. M. Kolb, Surf. Sci. **327**, L495 (1995).
[59] A. Morgante, K. C. Prince, G. Paolucci, and E. Tosatti, Surf. Sci. **199/200**, 621 (1987).
[60] G. Binnig, H. Rohrer, Ch. Gerber, and E. Weibel, Surf. Sci. **142**, L389 (1983).
[61] J. K. Gimzewski, R. Berndt, and R. R. Schlittler, Surf. Sci. **257**, 337 (1991); Phys. Rev. B **45**, 6844 (1992).
[62] M. Sturmat, R. Koch, and K. H. Rieder, Phys. Rev. Lett. **77**, 5071 (1996).
[63] R. Koch and M. Sturmat, Surf. Sci. **402–404**, 861 (1998).
[64] A thin layer of liquid *A* at the bottom of a vessel filled with a liquid *B* diffuses into *B*. Its concentration at a distance x from the bottom at the time t is $c(x,t) = (c_o/\sqrt[2]{\pi Dt})\exp(-x^2/4Dt)$.
[65] The intensity ratio has been calculated using the Ag(110) layer distance $d = 1.44$ Å, and an elastic mean free path of $\lambda = 5$ Å as found from SSC.
[66] J. D. Wrigley and G. Ehrlich, Phys. Rev. Lett. **44**, 661 (1980).
[67] G. L. Kellogg, Phys. Rev. Lett. **67**, 216 (1991).
[68] K. W. Jacobsen and J. K. Nørskov, Phys. Rev. Lett. **60**, 2496 (1988).
[69] Th. Michely, K. H. Besocke, and G. Comsa, Surf. Sci. **230**, L135 (1990).
[70] P. W. Palmberg and T. N. Rhodin, J. Chem. Phys. **49**, 134 (1968).